EPJ manuscript No.
(will be inserted by the editor)

arXiv:0805.4755v1 [astro-ph] 30 May 2008

(n,γ) Cross Sections of Light p Nuclei

Towards an Updated Database for the p Process

I. Dillmann[1,2], M. Heil[1], F. Käppeler[1], R. Plag[1], T. Rauscher[2], and F.-K. Thielemann[2]

[1] Institut für Kernphysik, Forschungszentrum Karlsruhe, Postfach 3640, D-76021 Karlsruhe, Germany
[2] Departement Physik und Astronomie, Universität Basel, Klingelbergstrasse 82, CH-4056 Basel, Switzerland

Received: date / Revised version: date

Abstract. The nucleosynthesis of elements beyond iron is dominated by the s and r processes. However, a small amount of stable isotopes on the proton-rich side cannot be made by neutron capture and are thought to be produced by photodisintegration reactions on existing seed nuclei in the so-called "p process". So far most of the p-process reactions are not yet accessible by experimental techniques and have to be inferred from statistical Hauser-Feshbach model calculations. The parametrization of these models has to be constrained by measurements on stable proton-rich nuclei. A series of (n,γ) activation measurements on p nuclei, related by detailed balance to the respective photodisintegrations, were carried out at the Karlsruhe Van de Graaff accelerator using the ^{7}Li(p,n)^{7}Be source for simulating a Maxwellian neutron distribution of kT= 25 keV. We present here preliminary results of our extended measuring program in the mass range between A=74 and A=132, including first experimental (n,γ) cross sections of ^{74}Se, ^{84}Sr, ^{120}Te and ^{132}Ba, and an improved value for ^{130}Ba. In all cases we find perfect agreement with the recommended MACS predictions from the Bao et al. compilation.

PACS. 25.40.Lw, 26.30.+k, 27.50.+e, 27.60.+j, 97.10.Cv

1 Introduction

Astrophysical models can explain the origin of most nuclei beyond the iron group in a combination of processes involving neutron captures on long (s process) or short (r process) time scales [1,2]. However, 32 stable, proton-rich isotopes between ^{74}Se and ^{196}Hg cannot be formed in that way. Those p nuclei are 10 to 100 times less abundant than the s and r nuclei in the same mass region. They are thought to be produced in the so-called γ or p process, where proton-rich nuclei are made by sequences of photodisintegrations and β^+ decays [3,4,5]. In this scenario, pre-existing seed nuclei from the s and r processes are destroyed by photodisintegration in a high-temperature environment, and proton-rich isotopes are produced by (γ,n) reactions. When (γ,p) and (γ,α) reactions become comparable or faster than neutron emission within an isotopic chain, the reaction path branches out and feeds nuclei with lower charge number Z. The decrease in temperature at later stages of the p process leads to a freeze-out via neutron captures and mainly β^+ decays, resulting in the typical p-process abundance pattern with maxima at ^{92}Mo (N=50) and ^{144}Sm (N=82).

The currently most favored astrophysical site for the p process is explosive burning in type II supernovae. The explosive shock front heats the outer O/Ne shell of the progenitor star to temperatures of 2-3 GK, sufficient for providing the required photodisintegrations. Following the nucleosynthesis in such astrophysical models, good agreement with the required p production is found, with exception of the low (A<100) and intermediate (150$\leq A\leq$ 165) mass range, which are underproduced by factors of 3-4 [6]. Currently, however, it is not yet clear whether the observed underproductions are due to a problem with astrophysical models or with the nuclear physics input, i.e. reaction rates. Thus, a necessary requirement towards a consistent understanding of the p process is the reduction of uncertainties in nuclear data. By far most of the several hundreds of required photodisintegration rates and their inverses need to be inferred from Hauser-Feshbach statistical model calculations [7,8]. Experimental data can improve the situation in two ways, either by directly replacing predictions with measured cross sections in the relevant energy range, or by testing the reliability of predictions at other energies when the relevant energy range is not experimentally accessible.

The role of (n,γ) reactions in the p process was underestimated for a long time, although it is obvious that they have an influence on the final p-process abundances. Neutron captures compete with (γ,n) reactions and thus hinder the photodisintegration flux towards light nuclei, especially at lower-Z isotopes and even-even isotopes in the vicinity of branching-points. Rayet et al. [9] have stud-

Send offprint requests to: iris.dillmann@ik.fzk.de

ied the influence of several components in their p-process network calculations. Their nuclear flow schemes show that branching points occur even at light p nuclei, and are shifted deeper into the proton-rich unstable region with increasing mass and temperature. In contradiction to Woosley and Howard [3], who claimed for their network calculations that (n,γ) can be neglected except for the lightest nuclei ($A\leq 90$), Rayet et al. also examined the influence of neutron reactions for temperatures between T_9= 2.2 and 3.2 GK by comparing overabundance factors if (n,γ) reactions on $Z>26$ nuclides are considered or completely suppressed. As a result, the overabundances were found to change by up to a factor 100 (for ^{84}Sr) if the (n,γ) channel was artificially suppressed. This rather high sensitivity indicates the need for reliable (n,γ) rates to be used in p-process networks.

The influence of a variation of reaction rates on the final p abundances has also been studied previously [10, 11]. It turned out that the p abundances are very sensitive to changes of the neutron-induced rates in the entire mass range, whereas the proton-induced and α-induced reaction rates are important at low and high mass numbers, respectively.

A third reason for the determination of neutron capture rates of p nuclei are those cases where experimental photodissociation rates are not accessible. The respective astrophysical photodisintegration rate can then be inferred from capture rates by detailed balance [12]. This is the case for most stable p nuclei, which are separated from stable isotopes by a radioactive nucleus. While the reaction rate ^{A}X$(\gamma,n)^{A-1}$X can be determined by bremsstrahlung [13], the reaction $^{A+1}$X$(\gamma,n)^{A}$X has to be measured via its inverse (n,γ) rate.

The present work comprises the first measurement of (n,γ) cross sections for the p-process isotopes ^{74}Se, ^{84}Sr, ^{120}Te and ^{132}Ba at kT= 25 keV, and a re-measurement of ^{130}Ba. The direct determination of stellar (n,γ) rates requires a "stellar" neutron source yielding neutrons with a Maxwell-Boltzmann energy distribution. We achieve this by making use of the ^{7}Li$(p,n)^{7}$Be reaction. In combination with the activation or time-of-flight technique, this offers a unique tool for comprehensive studies of (n,γ) rates and cross sections for astrophysics.

2 Experimental procedure

All measurements were carried out at the Karlsruhe 3.7 MV Van de Graaff accelerator using the activation technique. Neutrons were produced with the ^{7}Li$(p,n)^{7}$Be source by bombarding 30 μm thick layers of metallic Li on a water-cooled Cu backing with protons of 1912 keV, 30 keV above the reaction threshold. The resulting quasi-stellar neutron spectrum approximates a Maxwellian distribution for kT= 25.0 ± 0.5 keV [14]. Hence, the proper stellar capture cross section can be directly deduced from our measurement.

For all activations natural samples of the respective element were used. The selenium and tellurium samples were prepared from metal granules, whereas for the barium and strontium measurement thin pellets were pressed from powders of $Sr(OH)_2$, SrF_2, $SrCO_3$ and $BaCO_3$. In order to verify the stoichiometry, the powder samples were dried at 300°C and 800°C, respectively. All samples were enclosed in a 15 μm thick aluminium foil and sandwiched between 10-30 μm thick gold foils of the same diameter. In this way the neutron flux can be determined relative to the well-known capture cross section of ^{197}Au [14].

Throughout the irradiation the neutron flux was recorded in intervals of 1 min using a ^{6}Li-glass detector for later correction of the number of nuclei, which decayed during the activation. The activations were carried out with the Van de Graaff accelerator operated in DC mode with a current of ≈100 μA. The mean neutron flux over the period of the activations was $\approx 1.5\times 10^{9}$ n/s at the position of the samples, which were placed in close geometry to the Li target. The duration of the single activations varied between 3 h (for the partial cross section to ^{85}Sr^{m}, $t_{1/2}$= 67.6 m) and 130 h (for determination of the 10.52 y ground-state of ^{133}Ba).

3 Data analysis

The induced γ-ray activities were counted after the irradiation in a well defined geometry using a shielded Ge detector in a low background area. Energy and efficiency calibrations have been carried out with a set of reference γ-sources in the energy range between 60 keV and 2000 keV. For the counting of the long-lived ^{133}Ba^{g} activity ($t_{1/2}$= 10.52 y) two fourfold segmented Clover detectors in close geometry were used [15].

A detailed description of the analysis procedure is given in Refs. [18,19]. The number of activated nuclei A can be written as

$$A(i) = \Phi_{tot}\ N_i\ \sigma_i\ f_b(i), \tag{1}$$

where $\Phi_{tot} = \int \phi(t)dt$ is the time-integrated neutron flux and N_i the number of atoms in the sample. The factor f_b accounts for the decay of activated nuclei during the irradiation time t_a as well as for variations in the neutron flux. As our measurements are carried out relative to ^{197}Au as a standard, the neutron flux Φ_{tot} cancels out:

$$\frac{A(i)}{A(Au)} = \frac{\sigma_i\ N_i\ f_b(i)}{\sigma_{Au}\ N_{Au}\ f_b(Au)}$$
$$\Longleftrightarrow \sigma_i = \frac{A(i)\ \sigma_{Au}\ N_{Au}\ f_b(Au)}{A(Au)\ N_i\ f_b(i)}. \tag{2}$$

The reference value for the experimental ^{197}Au cross section in the quasi-stellar spectrum of the ^{7}Li$(p,n)^{7}$Be source is 586 ± 8 mb [14]. By averaging the induced activities of the gold foils, one can determine the neutron flux Φ_{tot} at the position of the sample and deduce the experimental cross section σ_i of the investigated sample as shown in Eq. 2.

Table 1. Decay properties of the product nuclei [16]. Isotopic abundances are from Ref. [17].

Reaction	Isot. abund. [%]	Final state	$t_{1/2}$	E_γ [keV]	I_γ [%]
^{74}Se(n,γ)^{75}Se	0.89 (0.04)	Ground state	119.79 ± 0.04 d	136.0	58.3 ± 0.7
				264.7	58.9 ± 0.3
^{84}Sr(n,γ)^{85}Sr	0.56 (0.01)	Ground state	64.84 ± 0.02 d	514.0	96 ± 4
		Isomer	67.63 ± 0.04 m	151.2 (EC)	12.9 ± 0.7
				231.9 (IT)	84.4 ± 2.2
^{120}Te(n,γ)^{121}Te	0.096 (0.001)	Ground state	19.16 ± 0.05 d	573.1	80.3 ± 2.5
		Isomer	154 ± 7 d	212.2 (IT)	81.4 ± 1.0
^{130}Ba(n,γ)^{131}Ba	0.106 (0.001)	Ground state	11.50 ± 0.06 d	123.8	29.0 ± 0.3
				216.1	19.7 ± 0.3
				373.2	14.0 ± 0.2
				496.3	46.8 ± 0.2
^{132}Ba(n,γ)^{133}Ba	0.101 (0.001)	Ground state	10.52 ± 0.13 y	356.0	62.1 ± 0.2
		Isomer	38.9 ± 0.1 h	275.9 (IT)	17.8 ± 0.6

4 Results and Discussion

4.1 General

In an astrophysical environment with temperature T, the neutron spectrum corresponds to a Maxwell-Boltzmann distribution

$$\Phi \sim E_n \; e^{-E_n/kT}. \tag{3}$$

The experimental neutron spectrum of the ^{7}Li(p,n)^{7}Be reaction approximates a Maxwellian distribution with kT= 25 keV almost perfectly [14]. But to obtain the exact Maxwellian averaged cross section $<\sigma>_{kT}=\frac{<\sigma\upsilon>}{\upsilon_T}$ for the temperature T, the energy-dependent cross section σ(E) has to be folded with the experimental neutron distribution to derive a normalization factor NF=$\frac{\sigma}{\sigma_{exp}}$. The normalized cross section in the energy range 0.01≤E$_n$≤4000 keV was used for deriving the proper MACS as a function of thermal energy kT:

$$\frac{<\sigma\upsilon>}{\upsilon_T} = <\sigma>_{kT} = \frac{2}{\sqrt{\pi}} \frac{\int_0^\infty \frac{\sigma(E_n)}{NF} \; E_n \; e^{-E_n/kT} \; dE_n}{\int_0^\infty E_n \; e^{-E_n/kT} \; dE_n}. \tag{4}$$

In this equation, $\frac{\sigma(E_n)}{NF}$ is the normalized energy-dependent capture cross section and E$_n$ the neutron energy. The factor υ_T= $\sqrt{2kT/m}$ denotes the most probable velocity with the reduced mass m.

Maxwellian averaged cross sections have to be corrected by a temperature-dependent stellar enhancement factor

$$SEF(T) = \frac{\sigma^{star}}{\sigma^{lab}}. \tag{5}$$

The stellar cross section σ^{star}=$\sum_\mu \sum_\nu \sigma^{\mu\nu}$ accounts for all transitions from excited target states μ to final states ν in thermally equilibrated nuclei, whereas the laboratory cross section σ^{lab}=$\sum_0 \sum_\nu \sigma^{0\nu}$ includes only captures from the target ground state. In the investigated cases the thermal population effects in the stellar plasma at p-process temperatures are small for Se and Sr, but increase up to 1.42 for Te and Ba (Table 2).

Table 2. Stellar enhancement factors for different temperatures [12].

T [GK]	kT [keV]	SEF ^{74}Se	SEF ^{84}Sr	SEF ^{120}Te	SEF ^{130}Ba	SEF ^{132}Ba
0.3	26	1.00	1.00	1.00	1.00	1.00
2.0	172	1.01	1.02	1.10	1.23	1.16
2.5	215	1.02	1.06	1.18	1.33	1.22
3.0	260	1.03	1.09	1.25	1.42	1.28

4.2 Experimental results

For sample characteristics, activation features, and a detailed discussion of the Se and Sr results see Ref. [19]. The results of the Te and Ba measurements in this paper are yet preliminary and correspond only to the cross sections derived with the experimental neutron distribution at kT= 25 keV. Nevertheless, this value approximates the Maxwellian averaged cross section at kT= 30 keV very well and can be used for comparison with other stellar cross sections. The resulting MACS at 30 keV (for Se and Sr) and the experimental values for Te and Ba are shown in Table 3. The extrapolation to higher (p-process) temperatures will not be discussed here and can also be found in Ref. [19].

4.2.1 ^{74}Se(n,γ)^{75}Se

The ^{74}Se(n,γ)^{75}Se reaction was analyzed via the two strongest transitions in ^{75}As at 136.0 keV and 264.7 keV. The capture cross section derived with the experimental neutron distribution is 281 ± 15 mb. The result for the stellar cross section is $<\sigma>_{30}$= 271 mb, in perfect agreement with the previously estimated value of 267 ± 25 mb from Ref. [20].

4.2.2 ^{84}Sr(n,γ)^{85}Sr^{g,m}

In case of ^{84}Sr, neutron captures populate both, ground and isomeric state of ^{85}Sr. While ^{85}Sr^g decays can be identified via the 514 keV transition in ^{85}Rb, the decay of the

isomer proceeds mainly via transitions of 232 keV and 151 keV. The isomeric state is 239 keV above the ground state and decays either via a 7 keV- 232 keV cascade (internal transition, 86.6%) or directly by electron capture (13.4%) into the 151 keV level of the daughter nucleus.

The partial cross section to the isomeric state can be easily deduced from the above mentioned transitions at 151 keV and 232 keV and yields 189 ± 10 mb. The cross section to the ground state was measured to 112 ± 8 mb, which leads to a total capture cross section of 301 ± 17 mb.

The result for the total stellar cross section of ^{84}Sr is $<\sigma>_{30}$= 300 mb, 17 % lower than the 368 ±125 mb from Ref. [20]. The partial cross section to the isomer yields $<\sigma>_{30}$(part)= 190 mb.

4.2.3 ^{120}Te(n,γ)^{121}Te^{g,m}

The Te samples were analyzed via the 576 keV γ-line from the β^+ decay of ^{121}Te^g into ^{121}Sb. The partial cross section of the isomeric state cannot be measured directly after the irradiation due to a huge Compton background around 210 keV, but after a waiting time of 80 d the expected 212 keV from the IT to the ground state (88.6 %) could be determined.

The preliminary result for the neutron capture to the ground-state is 390 ± 16 mb, and 61 ± 2 mb for the partial cross section to the isomeric state. This leads to a (preliminary) total (n,γ) cross section of 451 ± 18 mb, which again is in good agreement with the estimated 420 ± 103 mb from Ref. [20].

4.2.4 ^{130}Ba(n,γ)^{131}Ba

The ^{130}Ba cross section can be determined via the transitions at 124 keV, 216 keV, 373 keV and 496 keV from the β^+ decay into ^{131}Cs. The resulting experimental cross section is 694 ± 20 mb, which exhibits a much smaller uncertainty than the 760 ± 110 mb from Ref. [21], which were derived at a filtered neutron beam.

4.2.5 ^{132}Ba(n,γ)^{133}Ba^{g,m}

The partial cross section to the 38.9 h isomer in ^{133}Ba was measured via the 276 keV line (IT) to be 33.6 ± 1.7 mb. The total capture cross section was determined with a Clover detector via the strongest EC decay transition into ^{133}Cs at 356.0 keV. The preliminary result is 368 ± 25 mb, in perfect agreement with the estimated 379 ± 137 mb from Ref. [20].

4.3 Comparison with theory

Fig. 1 shows a comparison of our experimental total capture cross sections with $<\sigma>_{30}$ values derived with various theoretical models [23,24,25,26,27,28,29,30]. For ^{74}Se and ^{84}Sr the experimental value shown is the MACS derived with the energy dependence of JEFF 3.0 [19,22], whereas the preliminary values for ^{120}Te, ^{130}Ba and ^{132}Ba shown here are only cross sections derived with the experimental neutron distribution.

In the case of ^{130}Ba our experimental value agrees with the measurement of Ref. [21]. In all other cases we find good agreement with the semi-theoretical values of Bao et al. [20], which are normalized NON-SMOKER cross sections accounting for known systematic deficiencies in the nuclear inputs of the calculation.

5 Summary

We have presented the results of an ongoing experimental program to determine more precise p-process reaction rates in the mass range A=70-140. The (n,γ) cross sections of the p nuclei ^{74}Se, ^{84}Sr, ^{120}Te, ^{132}Ba have been measured for the first time, including the partial cross sections to the isomeric states in ^{85}Sr, ^{121}Te, and ^{133}Ba. A re-measurement of ^{130}Ba yielded a more precise total cross section compared to the previous value [21].

As can be seen in Table 3, experimental Maxwellian averaged cross sections for ^{98}Ru, ^{102}Pd, ^{138}La, ^{158}Dy, ^{168}Yb, ^{174}Hf, ^{184}Os and ^{196}Hg are still missing. Thus, future efforts should be focussed on these measurements, as well as on an improvement of the accuracy of important isotopes like ^{92}Mo and ^{94}Mo.

6 KADoNiS- The Karlsruhe Astrophysical Database of Nucleosynthesis in Stars

The KADoNiS project is an online database for cross sections in the s process and p process (http://nuclear-astrophysics.fzk.de/k
Its first part consists of an updated version of the Bao et al. compilation [20] for cross sections relevant to the s process. A test launch of the KADoNiS webpage started in May 2005 with an online version of the original Bao et al. paper. By end of June 2005 the first updated version was online. For the six isotopes $^{128-130}$Xe, ^{147}Pm, ^{151}Sm and ^{180}Ta^m the previously recommended semi-theoretical MACS were replaced by first experimental results. More than 40 isotopes (a list is available online) exhibit new measurements, which were included to re-evaluate the recommended MACS.

The KADoNiS data sheets include all necessary information for the respective (n,γ) reaction (recommended total and partial cross sections, all available published values with references, energy dependence of the MACS for $5<kT<100$ keV, and the respective stellar enhancement factors).

The second part of KADoNiS is planned to be a collection of experimental p-process reaction rates, including (n,γ), (p,γ), (α,γ) and their respective photodissociation rates. The projected launch of this part of the database will be December 2005.

Table 3. Maxwellian averaged cross sections $<\sigma>_{30}$ of all 32 *p*-process nuclei at kT= 30 keV. Values taken from this work are in bold. ([1]) Relative to Si ≡ 10^6. ([2]) Rescaled NON-SMOKER cross sections accounting for known systematic deficiencies in the nuclear inputs [20]. ([3]) Xe abundances taken from Ref. [33]. ([4]) Modified values [30]. ([5]) Preliminary cross section.

Isotope	Solar Abundance([1])		Hauser-Feshbach prediction [mb]		Recommended
	Anders [31]	Lodders [32]	MOST [29]	NON-SMOKER [28]	values [mb] [20]
^{74}Se	5.50×10^{-1}	5.80×10^{-1}	304	207	**271 ± 15**
^{78}Kr	1.53×10^{-1}	2.00×10^{-1}	344	351	312 ± 26
^{78}Kr$\rightarrow^m$					92.3 ± 6.2
^{84}Sr	1.32×10^{-1}	1.31×10^{-1}	296 ([4])	393	**300 ± 17**
^{84}Sr$\rightarrow^m$					**190 ± 10**
^{92}Mo	3.78×10^{-1}	3.86×10^{-1}	44	128	70 ± 10
^{94}Mo	2.36×10^{-1}	2.41×10^{-1}	87	151	102 ± 20
^{96}Ru	1.03×10^{-1}	1.05×10^{-1}	291	281	207 ± 8
^{98}Ru	3.50×10^{-2}	3.55×10^{-2}	370	262	173 ± 36 ([2])
^{102}Pd	1.42×10^{-2}	1.46×10^{-2}	1061	374	373 ± 118 ([2])
^{106}Cd	2.01×10^{-2}	1.98×10^{-2}	434	451	302 ± 24
^{108}Cd	1.43×10^{-2}	1.41×10^{-2}	260	373	202 ± 9
^{113}In	7.90×10^{-3}	7.80×10^{-3}	413	1202	787 ± 70
^{113}In$\rightarrow^m$					480 ± 160
^{112}Sn	3.72×10^{-2}	3.63×10^{-2}	208	381	210 ± 12
^{114}Sn	2.52×10^{-2}	2.46×10^{-2}	106	270	134.4 ± 1.8
^{115}Sn	1.29×10^{-2}	1.27×10^{-2}	212	528	342.4 ± 8.7
^{120}Te	4.30×10^{-3}	4.60×10^{-3}	340 ([4])	551	**451 ± 18**([5])
^{120}Te$\rightarrow^m$					**61 ± 2**([5])
^{124}Xe	5.71×10^{-3}	6.57×10^{-3} ([3])	593	799	644 ± 83
^{124}Xe$\rightarrow^m$					131 ± 17
^{126}Xe	5.09×10^{-3}	5.85×10^{-3} ([3])	472	534	359 ± 51
^{126}Xe$\rightarrow^m$					40±6
^{130}Ba	4.76×10^{-3}	4.60×10^{-3}	561	730	**694 ± 20**([5])
^{132}Ba	4.53×10^{-3}	4.40×10^{-3}	300	467	**368 ± 25**([5])
^{132}Ba$\rightarrow^m$					**33.6 ± 1.7**([5])
^{136}Ce	2.16×10^{-3}	2.17×10^{-3}	227	495	328 ± 21
^{136}Ce$\rightarrow^m$					28.2 ± 1.6
^{138}Ce	2.84×10^{-3}	2.93×10^{-3}	160	290	179 ± 5
^{138}La	4.09×10^{-3}	3.97×10^{-3}	194	767	
^{144}Sm	8.00×10^{-3}	7.81×10^{-3}	37	209	92 ± 6
^{156}Dy	2.21×10^{-3}	2.16×10^{-3}	2025	1190	1567 ± 145
^{158}Dy	3.78×10^{-3}	3.71×10^{-3}	2188	949	1060 ± 400 ([2])
^{162}Er	3.51×10^{-3}	3.50×10^{-3}	1818	1042	1624 ± 124
^{168}Yb	3.22×10^{-3}	3.23×10^{-3}	917	886	1160 ± 400 ([2])
^{174}Hf	2.49×10^{-3}	2.75×10^{-3}	709	786	956 ± 283 ([2])
^{180}W	1.73×10^{-3}	1.53×10^{-3}	722	707	536 ± 60
^{184}Os	1.22×10^{-3}	1.33×10^{-3}	697	789	657 ± 202 ([2])
^{190}Pt	1.70×10^{-3}	1.85×10^{-3}	659	760	677 ± 82
^{196}Hg	4.80×10^{-3}	6.30×10^{-3}	493	372	650 ± 82 ([2])

References

1. E.M. Burbidge, G.R. Burbidge, W.A. Fowler, F. Hoyle, Rev. Mod. Phys. **29**, 547 (1957).
2. K. Langanke, M. Wiescher, Rep. Prog. Phys. **64**, 1657 (2001).
3. S.E. Woosley, W.M. Howard, Astrophys. J. Suppl. Ser. **36**, 285 (1978).
4. S.E. Woosley, W.M. Howard, Astrophys. J. **354**, L21 (1990).
5. M. Rayet, M. Arnould, M. Hashimoto, N. Prantzos, K. Nomoto, Astron. Astrophys. **298**, 517 (1995).
6. T. Rauscher, A. Heger, R.D. Hoffman, S.E. Woosley, Astrophys. J. **576**, 323 (2002).
7. W. Hauser, H. Feshbach, Phys. Rev. **87**, 366 (1952).
8. T. Rauscher, F.-K. Thielemann, H. Oberhummer, Astrophys. J. **451**, L37 (1995).
9. M. Rayet, N. Prantzos, M. Arnould, Astron. Astrophys. **227**, 271 (1990).
10. T. Rauscher, Nucl. Phys. A **758**, 549c (2005).
11. W. Rapp, Report FZKA **6956**, Forschungszentrum Karlsruhe, (2004).
12. T. Rauscher, F.-K. Thielemann, At. Data Nucl. Data Tables **75**, 1 (2000).
13. K. Vogt, P. Mohr, M. Babilon, J. Enders, T. Hartmann, C. Hutter, T. Rauscher, S. Volz, A. Zilges, Phys. Rev. C **63**, 055802 (2001).
14. W. Ratynski, F. Käppeler, Phys. Rev. C **37**, 595 (1988).

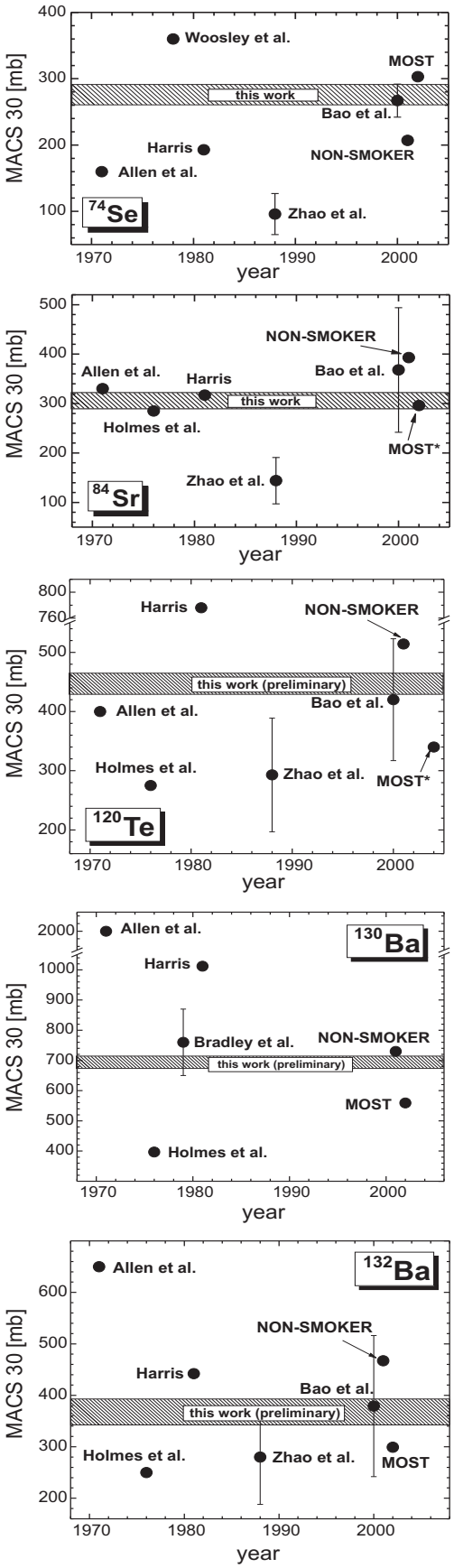

Fig. 1. Comparison of MACS30 predictions. MOST* marks modified values [30].

15. S. Dababneh, N. Patronis, P.A. Assimakopoulos, J. Görres, M. Heil, F. Käppeler, D. Karamanis, S. O'Brien, R. Reifarth, Nucl. Instrum. Meth. A **517**, 230 (2004).
16. National Nuclear Data Center, www.nndc.bnl.gov/nudat2, (2004).
17. K.J.R. Rosman, P.D.P. Taylor, Pure and Applied Chemistry **70**, 217 (1998).
18. H. Beer, F. Käppeler, Phys. Rev. C **21**, 534 (1980).
19. I. Dillmann, M. Heil, F. Käppeler, T. Rauscher, F.-K. Thielemann, to be published in Phys. Rev. C, (2005).
20. Z.Y. Bao, H. Beer, F. Käppeler, F. Voss, K. Wissshak, T. Rauscher, At. Data Nucl. Data Tables **76**, 70 (2000).
21. T. Bradley, Z. Parsa, Nuclear Cross Sections for Technology, edited by J.L. Fowler, C.H. Johnson and C.D. Bowman (National Bureau of Standards, Washington D.C.), 344 (1979).
22. NEA, Joint Evaluated Fission and Fusion General Purpose File: JEFF 3.0; Online: www.nea.fr/html/dbdata/eva/evaret.cgi, (2004).
23. B. Allen, J. Gibbons, R. Macklin, Adv. Nucl. Phys. **4**, 205 (1971).
24. J. Holmes, S.E. Woosley, W. Fowler, B. Zimmerman, At. Data Nucl. Data Tables **18**, 305 (1976).
25. S.E. Woosley, W. Fowler, J. Holmes, B. Zimmerman, At. Data Nucl. Data Tables **22**, 371 (1978).
26. M. Harris, Astrophys. Space Sci. **77**, 357 (1981).
27. Z. Zhao, D. Zhou, D. Cai, Nuclear Data for Science and Technology, edited by S. Igarasi (Saikon, Tokyo), 513 (1988).
28. T. Rauscher, F.-K. Thielemann, At. Data Nucl. Data Tables **79**, 47 (2001).
29. S. Goriely, Hauser-Feshbach rates for neutron capture reactions (version 09/12/02), http://www-astro.ulb.ac.be/Html/hfr.html.
30. S. Goriely, private comm., (2005).
31. E. Anders, N. Grevesse, Geochim. Cosmochim. Acta **53**, 1997 (1989).
32. K. Lodders, Astrophys. J. **591**, 1220 (2003).
33. R. Reifarth, M. Heil, F. Käppeler, F. Voss, K. Wisshak, Phys. Rev. C **66**, 064603 (2002).